Algorithm Theoretical Basis for Himawari-8 Cloud Mask Product

IMAI Takahito* and YOSHIDA Ryo**

Abstract

This paper describes the algorithm theoretical basis for the Himawari-8 Cloud Mask Product (CMP) developed by the Meteorological Satellite Center. CMP is part of the Fundamental Cloud Product, which incorporates cloud phase, type and top altitude from Himawari-8/AHI and has been operational since 7 July 2015.

The CMP algorithm is based on the cloud mask technique of NWC-SAF for MSG/SEVIRI and NOAA/NESDIS for GOES-R/ABI. Most cloud detection tests involve threshold methods based on radiative transfer calculation using NWP data as atmospheric profiles. The thresholds are modified using offsets determined on the basis of comparison with the MODIS cloud mask product. Initial results showed that the CMP hit ratio derived from such comparison was more than 85%. The CMP algorithm was applied to SEVIRI data, with results showing hit ratios with the MODIS product were around 85% for all seasons.

1. Introduction

Himawari-8 is the new geostationary satellite of the Japan Meteorological Agency (JMA). It was launched on 7 October 2014 and began operation on 7 July 2015. The satellite carries the Advanced Himawari Imager (AHI), which is greatly improved over past imagers in terms of its number of bands and its temporal/special resolution (Bessho et al. 2016). Using AHI data, JMA's Meteorological Satellite Center (MSC) developed the Himawari-8 Cloud Mask Product (CMP).

Cloud mask is used to discriminate cloudy pixels from clear ones in satellite data. Numerous satellite products require cloud mask information. By way of example, Sea Surface Temperature (SST) (Yasuda and Shirakawa 1999), Clear Sky Radiance (CSR) (Uesawa 2009) and Aerosol Detection (Okawara et al. 2003) are derived in clear pixels. Conversely, Cloud Grid Information (Tokuno 2002) is processed in cloudy pixels.

There were no MSC cloud mask products before the start of Himawari-8's operation; each satellite product had its own cloud mask process. As cloud mask is also required for most Himawari-8 products, MSC decided to develop CMP as a resource available for Himawari-8 products in common. CMP is a part of the Fundamental Cloud Product (FCP), which contains cloud phase, type and top height for Himawari-8/AHI pixels (Mouri et al. 2016a, 2016b). FCP has been produced since Himawari-8

began operation.

This paper describes the algorithm theoretical basis for CMP.

2. Algorithm

2.1 Overview

Cloud detection in the CMP algorithm is based on comparison of observation data and clear sky data calculated from numerical weather prediction (NWP) data. If observation data differ from clear sky data, the pixel is cloudy. To discriminate between cloudy and clear pixels, it is desirable for observation variables in clear and cloudy conditions to differ and for the physical reason behind the difference to be explicit (e.g., temperature, reflectance and emissivity of the top and transmittance relating to clouds and the atmosphere). Rather than encompassing retrieval of these five variables, most of the tests in the CMP algorithm involve the use of brightness temperature or reflectance data with similar tendencies. Cloud mask tests are based on the cloud mask algorithm of the NoWCasting (NWC) Satellite Application Facility (SAF) (Meteo-France, 2012) and the National Oceanic and Atmospheric Administration (NOAA)/National Environmental Satellite, Data, and Information Service (NESDIS) (Heidinger and Straka III, 2012).

Radiative transfer calculation using NWP for

* Office of Observation Systems Operation, Observation Department, Japan Meteorological Agency
** System Engineering Division, Data Processing Department, Meteorological Satellite Center

atmospheric profiles is essentially adopted for estimation of clear sky data. As the quality of results obtained from such calculation are not always high enough for use in cloud detection thresholds, offsets are introduced as additional threshold terms.

In addition to numerous cloud detection tests, the CMP algorithm also includes snow/sea ice detection tests, aerosol detection tests and filters. The algorithm is outlined in Fig. 1.

First, a snow/sea ice detection step is performed. If snow or sea ice is detected, the pre-final cloud mask based on the results of all the cloud detection tests is set to clear. For pixels where no snow or sea ice is detected, a series of cloud detection tests is performed. If cloud is detected in any of these, the pre-final cloud mask is set to cloudy. Pixels determined as cloudy in top temperature or reflectance tests can be modified as clear based on the outcomes of atmospheric absorption tests. A filter is applied for the pre-final cloud mask, and cloudy pixels are divided into cloudy and clear-cloudy mixed pixels in the filter process. The CMP algorithm includes aerosol detection based on an ash detection algorithm (Pavolonis et al. 2009). The final cloud mask is generated by combining the cloud mask results with those of aerosol detection.

2.2 Data

2.2.1 Input data

The inputs for the CMP algorithm are Himawari Standard Data (HSD), the results of radiative transfer calculation, NWP data and surface condition data.

AHI has 16 bands (B01 – B16) with different spatial resolutions as shown on the left of Table 1. HSD full-disk data consist of 22,000 x 22,000 pixels for B03, 11,000 x 11,000 pixels for B01, B02 and B04, and 5,500 x 5,500 pixels for the other bands. The size of each pixel for infrared bands (B05 – B16) corresponds to 2 x 2 pixels for B01, B02 and B04 and 4 x 4 pixels for B03. The CMP algorithm is applied to each infrared pixel (5,500 x 5,500). Cloud mask operation involves the use of data from the current situation as well as data from 10 and 60 minutes ago to enable calculation of temporal variations in variables for the cloud mask test. AHI data for CMP are summarized on the right of Table 1. The CMP algorithm requires brightness temperature T_λ, reflectance R_λ^{org} and radiation intensity data I_λ from HSD, where λ denotes center wavelength of the band.

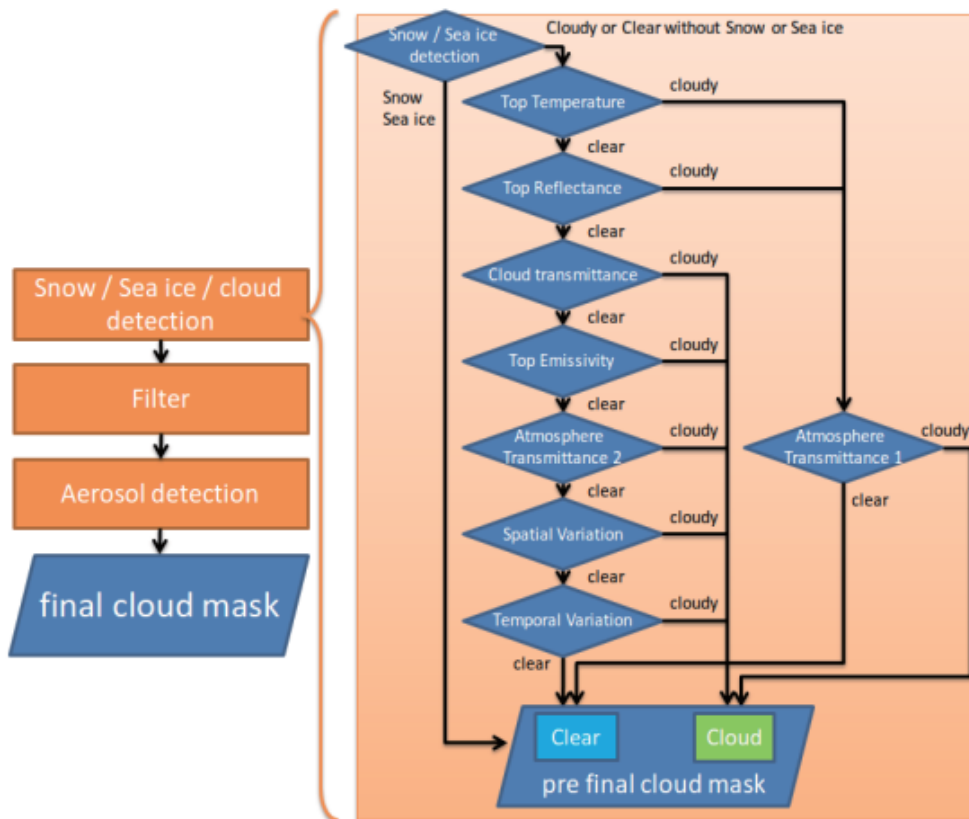Radiative transfer calculation-based data required for CMP are listed in Table 2.

Fig.1 CMP algorithm outline

Table 1 Specifications of AHI bands and data required for CMP

Band	Center wavelength [μm]	Spatial resolution at sub satellite point [km]	Timing of data used		
			60 min. ago	10 min. ago	Current
B01	0.47	1.0			
B02	0.51	1.0			
B03	0.64	0.5		*	*
B04	0.86	1.0			*
B05	1.6	2.0			*
B06	2.3	2.0			
B07	3.9	2.0			*
B08	6.2	2.0			
B09	6.9	2.0			
B10	7.3	2.0			*
B11	8.6	2.0	*		*
B12	9.6	2.0			
B13	10.4	2.0	*	*	*
B14	11.2	2.0			*
B15	12.4	2.0	*		*
B16	13.3	2.0			

Table 2 Data based on radiative transfer calculation

Band	Surface	Clear sky data for atmosphere top	Black body radiance for tropopause	Rough estimation of cloud top radiance
B03	Sea/land	R_λ^{srf}		
B04	Sea			
B05	Sea/snow			
B07	Sea/land	$T_\lambda^{srf}, I_\lambda^{srf}$		
B10	Sea/land		*	
B11	Sea/land		*	
B13	Sea/land			
B14	Sea/land		*	*
B15	Sea/land		*	*

Reflectance R_λ^{srf} for the top of the atmosphere (TOA) with clear sky conditions is used as reflective band (B03, B04 and B05) data. Reflectance is estimated using look-up table (LUT) values calculated from RSTAR (Nakajima and Tanaka 1986) with NWP data using the latest forecast values from JMA's Global Spectral Model (GSM) and the surface bidirectional reflectance distribution function (BRDF). Sea surface BRDF $R_\lambda^{CoxMunk}$ is calculated following Cox and Munk (1954) using RSTAR with GSM-predicted surface horizontal wind. Land surface BRDF is calculated using the Roujean model (Roujean et al. 1992) with the Moderate Resolution Imaging Spectroradiometer (MODIS) BRDF product (Strahler et al. 1999). In snow surface conditions, an LUT calculated using the ARTMASS radiative transfer model (Aoki et al. 1999) is used.

Brightness temperature T_λ^{srf} and radiance I_λ^{srf} at the TOA are used as infrared band (B07, B10, B11, B13, B14 and B15) data. In addition to clear sky condition data, radiance calculated for conditions with black body (BB) cloud on the tropopause I_λ^{trp} and for roughly estimated cloud top radiance I_λ^{opq} are used for aerosol detection. Estimation of I_λ^{opq} is based on Pavolonis et al. (2009). For radiative transfer calculation, the fast radiative transfer model known as RTTOV (Radiative Transfer for the Television and Infrared Observation Satellite (TIROS) Operational Vertical Sounder; Eyre 1991) with NWP data from the GSM is used.

Merged satellite and in situ data for the global daily sea surface temperature (MGDSST; Kurihara et al. 2006) are used for sea-surface cloud detection tests. JMA's internal snow and sea ice cover products are used for

snow/sea surface classification.

In addition, the following geographical data for individual pixels are used: sun zenith angle θ_{sunZ}, sun azimuth angle θ_{sunA}, satellite zenith angle θ_{satZ}, satellite azimuth angle θ_{satA}, sunlight scattering angle at the surface or cloud θ_{scat} and altitude z. Angles are given in degrees unless otherwise stated.

2.2.2 Output data

CMP provides information on whether pixels are clear, cloudy or clear-cloudy mixed along with quality information (high/low) and aerosol information for each pixel (Table 3). As the CMP algorithm is applied to each infrared pixel, CMP output consists of 5,500 x 5,500 pixels for each full-disk scene. The specifications of CMP are given in Table 4.

2.2.3 Operators and processed data

This subsection summarizes operators and processed data used in CMP.

Processed data

R_λ^{mod}: R_λ^{org} with sun zenith angle correction (Li and Shibata 2006)

$\varepsilon_\lambda^{stropo}$: effective emissivity of single-layer cloud on the tropopause (EST), which essentially has the same tendency as brightness temperature. The spatial continuity of the EST field is superior to that of the brightness temperature field because the effects of the surface and the atmosphere are reduced by combining observation data and estimated data. The definition is as follows:

$$\varepsilon_\lambda^{stropo} = \frac{I_\lambda - I_\lambda^{srf}}{I_\lambda^{trp} - I_\lambda^{srf}} \tag{1}$$

$\varepsilon_\lambda^{sopaque}$: effective emissivity of single-layer cloud on the roughly estimated cloud top level in a single-layer situation. The definition is as follows:

$$\varepsilon_\lambda^{sopaque} = \frac{I_\lambda - I_\lambda^{srf}}{I_\lambda^{opq} - I_\lambda^{srf}} \tag{2}$$

β_λ^{stropo}, $\beta_\lambda^{sopaque}$: beta ratio of $\varepsilon_\lambda^{stropo}$ and $\varepsilon_\lambda^{sopaque}$. The definition of the beta ratio is as follows:

$$\beta_{\lambda_1/\lambda_2}^{x} = \frac{\ln(1 - \varepsilon_{\lambda_1}^{x})}{\ln(1 - \varepsilon_{\lambda_2}^{x})}, \tag{3}$$

where x denotes stropo or sopaque.

Operators

$STAT_8(v)$: statistical value of the dataset on the eight pixels (infrared size) surrounding the cloud masking pixel, where STAT is replaced by SD for standard deviation, MAX for the maximum value, MIN for the minimum value and MEAN for the mean value. Only data on pixels with the same surface condition (sea/land) as that of the cloud masking pixels can contribute to statistical values.

$CORR(v_1, v_2)$: coefficient of correlation between the dataset of variable v1 and variable v2 in a 5 x 5-pixel segment centered on the cloud masking pixel

$STAT_{CMA}(v)$: statistical value of the dataset on high-resolution pixels in a cloud masking pixel, where STAT is replaced by SD for standard deviation, MAX for the maximum value, MIN for the minimum value and

Table 3 Summary of CMP output. "HQ" and "LQ" denote quality information (high and low). "Mixed" represents clear-cloudy mixed. The numbers in the table are assigned for each pixel in the output.

	Clear (HQ)	Clear (LQ)	Mixed (HQ)	Mixed (LQ)	Cloudy (HQ)	Cloudy (LQ)
No aerosol	0	1	10	11	20	21
Aerosol (HQ)	50	51	60	61	70	71
Aerosol (LQ)	55	56	65	66	75	76

Table 4 CMP specifications

Area	70°S to 70°N, 70°E to 150°W
Spatial resolution	Infrared pixels in HSD (2 km at SSP)
Frequency	Hourly
Projection method	Normalized Geostationary Projection (as per HSD)

MEAN for the mean value. 4 x 4 original B03 data and 2 x 2 original B01, B02, B04 data are included in the cloud masking pixel. Due to its frequent appearance in this paper, $MEAN_{CMA}(R_\lambda^{org})$ is expressed simply as R_λ.

ABS(v): absolute value of the variable v

NWC(v): value of the variable v on the neighboring warmest center (NWC), which is the pixel with the highest $T_{10.4}$ value and the same surface condition in a 21 x 21-pixel segment centered on the cloud masking pixel. The surface condition is classified as either sea or land in NWC calculation. The optical depth of the NWC is the thinnest among its neighbors. The NWC is expected to be clear or to have thinner cloud than the cloud masking pixel.

LRC(v): value of the variable v on the local radiative center (LRC), which is the nearest local maximum of the $\varepsilon_{11.2}^{stropo}$ field from the cloud masking pixel. If the cloud masking pixel is cloudy, the LRC is the highest or thickest cloud pixel in the cloud cluster to which the cloud masking pixel belongs. If the LRC is cloudy, the cloud masking pixel is likely to be cloudy in consideration of spatial continuity. In contrast, if the LRC is clear, the cloud masking pixel is also likely to be clear.

Δ_t**(v)**: temporal difference of variable v. $\left. v \right|_{t_0} - \left. v \right|_{t_0 - t}$

max(v₁, v₂,…,vₙ): maximum value of v_1, v_2, ..., v_n

2.3 Scene classification

In some cloud mask tests, thresholds and equations depending on geometric and surface conditions are required.

Based on geometric conditions, pixels are classified as day ($\theta_{sunZ} < 85$), night ($\theta_{sunZ} > 93$), twilight ($85 \le \theta_{sunZ} \le 93$) or sunglint ($\theta_{sunZ} < 75$ and $0.1 < R_{0.64}^{CoxMunk}$).

Based on surface conditions, pixels are first classified as sea, land, snow, sand or vegetation. Snow pixels are those in which snow or sea ice has been detected in the last four days. For the polar night area, JMA's snow and sea ice cover products are used for snow classification. Based on Black Sky Albedo (BSA) R_λ^{BSA} estimated using the MODIS BRDF product (Strahler et al. 1999), land ($0.1 \le R_{0.64}^{BSA} \le 0.3$), sand ($0.3 \le R_{0.64}^{BSA}$) and vegetation ($R_{0.64}^{BSA} < 0.1$) are distinguished. Four types of surfaces are then identified: 1: Coast pixels: those in sea areas near land/snow/sand/vegetation pixels or land/snow/sand/vegetation pixels near sea pixels; 2: snow neighbor pixels: those centered in a 16 x 16-pixel segment containing 5 snow pixels; 3: cold surface pixels: those with a low surface temperature ($T^{srf} < 263$ K or $T^{srf} < 268$ K in snow neighbor pixels) and a low altitude ($z < 1,500$ m); and 4: mountain pixels: those centered in 3 x 3-pixel segments with a high standard deviation of altitude ($SD_8((z_{center}-z) \times dT / dz) > 1.0$, where z_{center} denotes the altitude of the center pixel).

2.4 Cloud mask tests

2.4.1 Snow/sea ice detection

Discrimination between cloud and clear sky over snow/sea ice with a single test is challenging because most observation variables have similar values for both conditions. Accordingly, a number of tests involving top reflectance, top temperature and cloud transmittance are applied simultaneously. As top reflectance tests are essential, snow/sea ice detection is performed for pixels with a sun zenith angle of less than 85.0 degrees. If all of the following conditions are satisfied, the pixel is marked as clear sky over a snow surface:

$$R_{1.6} < R_{1.6}^{srf} \tag{4}$$

$$NDWI = \frac{R_{0.64} - R_{1.6}}{R_{0.64} + R_{1.6}} > 0.3 + 0.15 \cdot \{\cos(\theta_{scat}) + 1\}^2 \tag{5}$$

$$\frac{T_{3.9} - T_{10.4}}{\cos(\theta_{sunZ})} < 10.0 \tag{6}$$

$$T_{10.4}^{srf} - 5.0 < T_{10.4} < 286.15 \tag{7}$$

$$T_{10.4} - T_{12.4} < 2.0 \tag{8}$$

$$R_{0.64} > R_{0.64}^{srf} \quad or \quad R_{0.64} > 0.2 + 0.45 \cdot \{\cos(\theta_{scat}) + 0.55\}^2 \tag{9}$$

$$R_{0.86} > 0.2 \tag{10}$$

Here, NDWI denotes Normalized Differential Water Index.

For detection of clear sky over sea ice, the following conditions are used:

$$SST^{anal} < 277.15 \tag{11}$$

$$R_{1.6} < R_{1.6}^{srf} \tag{12}$$

$$NDWI > 0.3 + 0.15 \cdot \{\cos(\theta_{scat}) + 1\}^2 \tag{13}$$

$$T_{10.4}^{srf} - 5.0 < T_{10.4} < 277.15 \qquad (14)$$

$$T_{10.4} - T_{12.4} < 2.0 \qquad (15)$$

$$R_{0.64} > R_{0.64}^{srf} \qquad (16)$$

$$R_{0.86} > 0.2 \qquad (17)$$

Here, SST^{anal} is the MGDSST (Kurihara et al. 2006).

2.4.2 Top temperature tests

If the observed top temperature is lower than the clear sky value, the pixel is considered to be cloudy because the target of CMP is cloud in the troposphere, where the upper atmosphere is essentially colder than the lower atmosphere. If the following condition is satisfied for land, sand and vegetation pixels, the pixel is marked as cloudy:

$$T_{10.4} < T_{10.4}^{srf} + dT_{10.4}^{elv} + dT_{10.4}^{cool} + offset \qquad (18)$$

Here, $dT_{10.4}^{elv}$ represents correction for the altitude difference between the NWP model (z_{NWP}) and the actual value. For snow neighbor pixels, $dT_{10.4}^{cool}$ is used to offset the difficulty of expression for extremely cool land at night in the NWP model. The expressions are as follows:

$$dT_{10.4}^{elv} = (z - z_{NWP}) \cdot \frac{dT}{dz} \qquad (19)$$

$$dT_{10.4}^{cool} = \begin{cases} -5.0 & ; 255K \leq T_{10.4}^{srf} \\ -5.0 - 0.4 \cdot (255 - T_{10.4}^{srf}) & ; T_{10.4}^{srf} < 255\,K \end{cases} \qquad (20)$$

Here, the temperature lapse rate of the international standard atmosphere (-6.49 [K/km]) is used for $\frac{dT}{dz}$.

For sea pixels, cloud detection condition is as follows:

$$SST < SST^{anal} + offset \qquad (21)$$

Here, SST is derived from an LUT using $T_{10.4}$, $T_{10.4} - T_{8.6}$, $T_{10.4} - T_{11.2}$, $T_{10.4}$, $-T_{12.4}$ and the satellite zenith angle.

Upper thick cloud can be easily detected using these tests, but thin cloud detection remains challenging due to relatively high brightness temperatures caused by the contribution of radiance from below the cloud.

2.4.3 Top reflectance tests

These tests leverage the tendency for the reflectance of cloud to be greater than those of land and sea surfaces. As determination of reflectance requires a certain level of sunlight, these tests are largely performed for day pixels. To reduce the effect of Rayleigh scattering, a band with a longer wavelength is desirable. If any of the following conditions is satisfied for sea pixels other than those with sunglint, the pixel is marked as cloudy:

$$R_{0.86} > R_{0.86}^{thr} + dR_{0.86}^{coast} + offset \qquad (22)$$

$$R_{1.6} > R_{1.6}^{thr} + dR_{1.6}^{coast} + offset \qquad (23)$$

Here, $dR_{\lambda}^{coast} = 0.03$ is a correction term added for coast pixels.

For land pixels, the cloud detection condition is as follows:

$$R_{0.64} > R_{0.64}^{srf} + dR_{0.64}^{coast} + dR_{0.64}^{fwd} + offset \qquad (24)$$

Here, $dR_{0.64}^{coast} = 0.03$ is a correction term added for coast pixels. $dR_{0.64}^{fwd}$ represents correction to offset the difficulty of $R_{0.64}^{srf}$ estimation when the sunlight scattering angle (θ_{scat}) at the surface is small.

$$dR_{0.64}^{fwd} = 0.04 + 0.29 \cdot [\cos(\theta_{scat}) + 0.68]^2 \qquad (25)$$

For sunglint pixels where sea surface reflectance is greater than that of cloud and gross testing is not effective, a reflectance ratio is used as follows:

$$R_{0.64} > 0.06 \qquad (26)$$

$$0 < \frac{1}{0.15} \frac{T_{3.9} - T_{10.4}}{\cos(\theta_{sunZ})} < R_{0.64} \qquad (27)$$

$$T_{3.9} < 320.0 \qquad (28)$$

In addition, a gross test of 3.9 μm reflectance is also used in water cloud detection for day and twilight pixels. If the following conditions are satisfied, the pixel is marked as cloudy:

$$T_{3.9} - T_{10.4} > T_{3.9-10.4}^{thr\_day} + offset \qquad (29)$$

$$T_{10.4} > 240.0 \qquad (30)$$

For sand pixels, the following condition is added to avoid erroneous detection:

$$T_{8.6} - T_{10.4} > -4.5 - 1.5 \cdot \left(\frac{1}{\cos(\theta_{satZ})} - 1 \right) \qquad (31)$$

where $T_{3.9-10.4}^{thr\_day}$ is the clear sky brightness temperature

difference for the daytime. The contribution from earth emissions and reflected sunlight is combined in the following expressions:

$$T_{3.9-10.4}^{thr\_day} = T_{3.9}^{srf} - T_{10.4}^{srf}$$
$$+ 0.7 \cdot R_{3.9}^{CoxMunk} \cdot \cos(\theta_{sunZ}) + 7.0 \qquad (32)$$

(over sea)

$$T_{3.9-10.4}^{thr\_day} = T_{3.9}^{srf} - T_{10.4}^{srf} + 0.4 \cdot R_{0.64}^{BSA} \cdot \cos(\theta_{sunZ})$$
$$+ 2.0 + 36.0 \cdot \cos(\theta_{sunZ}) \cdot \left[\cos(\theta_{scat}) - 0.41\right]^2 \qquad (33)$$

(over land)

These tests facilitate thick cloud detection for day pixels because thicker clouds are associated with higher reflectance of sunlight.

2.4.4 Top emissivity tests

These tests leverage emissivity differences between cloud and surfaces. To extract emissivity information from satellite data, brightness temperature differences between different bands are calculated. As upper cloud and daytime lower cloud can be easily detected using top temperature and reflectance tests, the targets of these tests are lower cloud at night and twilight pixels. For detection of lower cloud, it is desirable to use atmospheric window bands that have a variety of interaction tendency with cloud. Four brightness temperature difference tests are used.

The first is for vegetation pixels at night and twilight. If the following conditions are satisfied, the pixel is marked as cloudy:

$$T_{10.4} - T_{8.6} > 3.7 + \frac{0.3}{\cos(\theta_{satZ})} + offset \qquad (34)$$

$$\frac{1}{\cos(\theta_{satZ})} > 1.5 \qquad (35)$$

The second is for night pixels. The conditions are as follows:

$$T_{10.4} - T_{3.9} > T_{10.4}^{srf} - T_{3.9}^{srf} + offset \qquad (36)$$

$$T_{10.4} > 240.0 \qquad (37)$$

For sand, land or vegetation pixels, following condition is added to avoid erroneous detection:

$$T_{8.6} - T_{10.4} > -4.5 - 1.5 \cdot \left(\frac{1}{\cos(\theta_{satZ})} - 1\right) \qquad (38)$$

The third is for sea pixels at night. The conditions are as follows:

$$T_{12.4} - T_{3.9} > T_{12.4}^{srf} - T_{3.9}^{srf} + offset \qquad (39)$$

$$T_{10.4} > 240.0 \qquad (40)$$

The fourth is for sand pixels at night. The conditions are as follows:

$$T_{8.6} - T_{3.9} > T_{8.6}^{srf} - T_{3.9}^{srf} + offset \qquad (41)$$

$$T_{10.4} - T_{3.9} > T_{10.4}^{srf} - T_{3.9}^{srf} \qquad (42)$$

$$T_{10.4} > 240.0 \qquad (43)$$

2.4.5 Cloud absorption tests

Cirrus pixels are detected using the radiation absorption difference between different bands caused by clouds. As it is assumed in these tests that some radiation passes through the target cloud, thick cloud cannot be detected. Three brightness temperature difference tests are applied.

The first is for all pixels except the coast type. If the following conditions are satisfied, the pixel is marked as cloudy:

$$(T_{10.4} - T_{12.4}) > T_{10.4-12.4}^{thr} + offset \qquad (44)$$

$$SD_8(T_{10.4}) > 0.3 \qquad (45)$$

$$T_{10.4} < 310.0 \qquad (46)$$

$$T_{12.4}^{srf} < T_{10.4}^{srf} \qquad (47)$$

Here,

$$T_{10.4-12.4}^{thr} = \begin{cases} (T_{10.4}^{srf} - T_{12.4}^{srf}) \cdot \dfrac{T_{10.4} - 260.0}{T_{10.4}^{srf} - 260.0} & ; 270.0K \leq T_{10.4}^{srf} \\ 0 & ; T_{10.4}^{srf} < 270.0\,K \end{cases} \qquad (48)$$

The second is for all pixels. The conditions are as follows:

$$(T_{8.6} - T_{10.4}) > T_{8.6}^{srf} - T_{10.4}^{srf} + dT_{8.6-10.4}^{cool} + offset \qquad (49)$$

Here, $dT_{8.6-10.4}^{cool} = 0.4$ is a correction term for snow neighbor pixels with $T_{10.4}^{srf} < 250$ K.

The third is for night pixels. The conditions are as follows:

$$T_{3.9} - T_{10.4} > T_{3.9}^{srf} - T_{10.4}^{srf} + dT_{3.9-10.4}^{cool} + offset \qquad (50)$$

Here, $dT_{3.9-10.4}^{cool}$ is a correction term for snow neighbor pixels.

$$dT_{3.9-10.4}^{cool} = \begin{cases} \max(0, -(T_{3.9}^{srf} - T_{10.4}^{srf}) - 0.5 \cdot T_{10.4}^{srf} + 129.0) & ; 250 \le T_{10.4}^{srf} \le 255\,K \\ -(T_{3.9}^{srf} - T_{10.4}^{srf}) - 0.15 \cdot T_{10.4}^{srf} + 41.5 & ; T_{10.4}^{srf} < 250\,K \end{cases} \quad (51)$$

2.4.6 Atmospheric absorption tests

Clear pixels are detected using the radiation absorption difference between different bands caused by atmospheric conditions. Two brightness temperature difference tests are applied.

The first is for detection in relation to the inversion layer using bands with different sensitive altitudes. If the following conditions are satisfied, the pixel is marked as clear:

$$T_{7.3} - T_{10.4} > 0.5 \quad (52)$$

$$T_{10.4}^{srf} < 250.0 \quad (53)$$

This test is performed for pixels marked as cloudy based on top temperature or reflectance tests.

The second involves detection for very thick water vapor. As most water vapor is concentrated in the lowest layer of the troposphere, observation of significant water vapor indicates that the pixel is clear sky. If the following conditions are satisfied, the pixel is marked as cloudy:

$$T_{12.4} - T_{10.4} > T_{12.4}^{srf} - T_{10.4}^{srf} + offset \quad (54)$$

$$T_{12.4} - T_{10.4} > 1.5 \quad (55)$$

2.4.7 Spatial uniformity tests

In addition to scene-by-scene and pixel-by-pixel tests, spatial and temporal consistency tests are also performed.

Six tests involving spatial extent are used. Based on the tendency by which cloud top and the boundary between cloudy and clear areas is rougher than that of the ground or sea surface, cloud is detected using spatial variations of brightness temperature or reflectance.

The first is a brightness temperature test for sea pixels. If the following conditions are satisfied, the pixel is marked as cloudy:

$$SD_8(T_{10.4}) > 0.6 + offset \quad (56)$$

$$\frac{MAX_8(T_{10.4}) - T_{10.4}}{2} > noise(T_{10.4}) \quad (57)$$

Here, $noise(T_{10.4})$ represents sensor noise estimated from interpolation of Table 5, which gives brightness temperature calculated from the signal noise ratio (SNR) of radiance. If $T_{10.4}{}^{srf} > 240$, the following test is added:

$$SD_8(T_{10.4} - T_{3.9}) > \begin{cases} 0.2 & ; night / twilight \\ 0.4 & ; day \end{cases} \quad (58)$$

The second is a reflectance test for daytime sea pixels. The conditions are as follows:

$$SD_8(R_{0.86}) > 0.008 + 0.03 \cdot R_{0.86}^{srf} + offset \quad (59)$$

$$\frac{R_{0.86} - MIN_8(R_{0.86})}{2} > \frac{1}{SNR(I_{0.86})} \quad (60)$$

Here, $SNR(I_{0.86}) = 420$.

The third is a brightness temperature test for land pixels other than the mountain type. The conditions are as follows:

$$SD_8(T_{10.4}) > \begin{cases} 1.0 & ; night / twilight \\ 2.0 & ; day \end{cases} + offset \quad (61)$$

$$SD_8(T_{10.4} - T_{3.9}) > \begin{cases} 1.0 & ; night / twilight \\ 2.0 & ; day \end{cases} \quad (62)$$

The fourth is a reflectance test for daytime land pixels other than the mountain type. The conditions are as follows:

$$DR_{0.86} > f\left(\frac{DT_{10.4}}{DR_{0.86}}\right) + offset \quad (63)$$

Here,

$$Dv = \max(MAX_8(v) - v, v - MIN_8(v)) \quad (64)$$

and f(v) is estimated from interpolation of the values shown in Table 6.

Table 5 Sensor noise for different brightness temperatures

$T_{10.4}$[K]	250	260	270	280	290	300	310	320
$noise(T_{10.4})$[K]	0.0539	0.0583	0.0627	0.0674	0.0722	0.0772	0.0822	0.0875

Table 6 Variable dependency of threshold for cloud

V	-5	-3	0	0.25	0.5	1
f(v)	0.02	0.02	0.05	0.1	0.15	0.15

The fifth is a brightness temperature difference test for all pixels except the coast type. The conditions are as follows:

$$ABS[\{NWC(T_{10.4}) - NWC(T_{12.4})\} - (T_{10.4} - T_{12.4})] > offset \quad (65)$$

$$T_{10.4} - T_{12.4} < 1.0 \quad (66)$$

$$T_{10.4} < 300.0 \quad (67)$$

The sixth is a test of brightness temperature distribution correlation between the water vapor band and the window band for all pixels. The brightness temperature distribution of these bands has a tendency similar to that of spatial variation in thin upper cloud areas. The conditions are as follows:

$$CORR(T_{7.3}, T_{10.4}) > 0.7 \quad (68)$$

$$SD_8(T_{7.3}) > 0.5 \quad (69)$$

$$SD_8(T_{10.4}) > 0.5 \quad (70)$$

$$\frac{TPW}{\cos(\theta_{satZ})} > 0.3 \, cm \quad (71)$$

$$z < 2000 \, m \quad (72)$$

Here, TPW is total precipitable water in NWP data.

2.4.8 Temporal uniformity tests

Brightness temperature temporal variation tends to increase when a pixel changes from cloudy to clear or from clear to cloudy. Based on this tendency, two tests are applied.

The first involves brightness temperature drop within a 10-minute time frame. This corresponds to situations in which clear pixels change to cloudy or cloud rises or thickens as time advances. If the following conditions are satisfied, the pixel is marked as cloudy:

$$\Delta_{10}(T_{10.4}) < T^{thr}_{\Delta_{10}10.4} + offset \quad (73)$$

$$T_{10.4}\big|_{t_0} < 330.0 \quad (74)$$

$$T_{10.4}\big|_{t_0 - 10} < 330.0 \quad (75)$$

$$T^{srf}_{10.4}\big|_{t_0} < 330.0 \quad (76)$$

$$T^{srf}_{10.4}\big|_{t_0 - 10} < 330.0 \quad (77)$$

Here,

$$T^{thr}_{\Delta_{10}10.4} = \Delta_{10}(T^{srf}_{10.4}) \quad (78)$$

The second involves brightness temperature uniformity within a 60-minute time frame for twilight sea pixels that were cloudy 60 minutes previously. Figure 2 shows two-dimensional daytime frequency distribution for $\Delta_{60}T_{10.4}$ and $\Delta_{60}(T_{10.4}-T_{12.4})$ over sea. Both $\Delta_{60}T_{10.4}$ and $\Delta_{60}(T_{10.4}-T_{12.4})$ tend to be larger in (b) than in (a). Based on the results, pixels satisfying at least one of the conditions shown below remain cloudy. This condition results in correct identification of 96.9% of actually cloudy pixels and false identification 6.5% of actually clear pixels as cloudy.

$$\Delta_{60}(T_{10.4}) < 2.5 \quad (79)$$

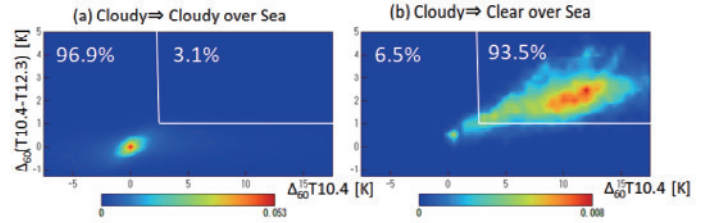$$\Delta_{60}(T_{10.4} - T_{12.4}) < 1.0 \quad (80)$$

Fig.2 Two-dimensional frequency distribution in terms of the daytime 60 min. temporal differences in $T_{10.4}$ ($\Delta_{60}T_{10.4}$) and $T_{10.4}$-$T_{12.4}$ ($\Delta_{60}(T_{10.4}-T_{12.4})$) over sea: (a) for pixels remaining cloudy; (b) for the pixels turning from cloudy to clear within the 60-minute period. The white line indicates the threshold of the test for twilight sea pixels, and numbers represent the cumulative frequency for each area.

For twilight land pixels, cloudy pixels cannot be discriminated using $\Delta_{60}(T_{10.4}-T_{12.4})$ as they can over land (Figure 3). However, using the following condition, 75.2% of actually cloudy pixels are correctly identified:

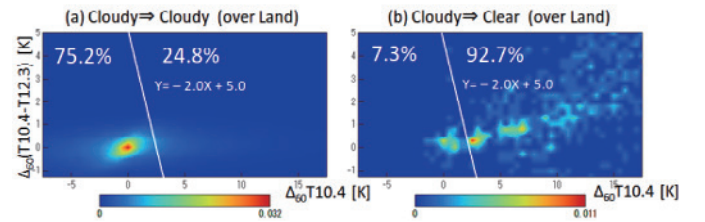$$\Delta_{60}(T_{10.4} - T_{12.4}) < -2.0\Delta_{60}T_{10.4} + 5.0 \quad (81)$$

Fig.3 As per Figure 2 but for results over land

2.4.9 Filters

Five filters are applied to the pre-final cloud mask in order to maintain its spatial continuity.

The first extends cloudy areas in twilight zones (75.0 deg. $< \theta_{sunZ} <$ 89.0 deg.). If clear pixels around cloudy pixels have a brightness temperature and reflectance similar to those of the cloudy pixels, the filter changes the clear pixels to cloudy. First, cloud clusters are created by combining adjacent cloudy pixels in the twilight area. For each cluster, the average brightness temperature $T_{10.4}^{AVE}$ and average reflectance with sun zenith angle correction $R_{0.64}^{modAVE}$ are calculated. If a clear pixel x adjacent to a pixel in a cloud cluster satisfies the following conditions, x is marked as cloudy:

$$\theta_{scat}\big|^x < 150 \tag{82}$$

$$MEAN_{CMA}(R_{0.64}^{\mod}\big|^x) > 1.05 \cdot R_{0.64}^{\mod AVE} \tag{83}$$

$$MEAN_{CMA}(R_{0.64}^{\mod}\big|^x) > 0.3 \tag{84}$$

$$T_{10.4}^{AVE} - 0.5 < T_{10.4}\big|^x \tag{85}$$

$$T_{10.4}\big|^x < T_{10.4}^{AVE} + 0.5 \tag{86}$$

For pixels adjacent to those set as cloudy after this filter's application, the above conditions are reapplied. If the conditions are newly satisfied for individual pixels, the cloudy area is extended accordingly.

The second filter changes coast pixels from cloudy to clear in order to correct misclassification resulting from spatial uniformity tests. If the following conditions are satisfied, the pixel is marked as clear:

- The pixel is cloudy as determined in spatial uniformity tests (Section 2.4.7).
- More than 10% of the eight surrounding pixels in a 3 x 3-pixel segment are clear.
- More than 50% of the 48surrounding pixels in a 7 x 7-pixel segment are clear.

The third filter changes snow neighbor pixels from clear to cloudy in order to correct misclassifications resulting from spatial uniformity tests. If the following conditions are satisfied, the pixel is marked as cloudy:

- The pixel is adjacent to a snow pixel.
- The pixel is cloudy as determined in spatial uniformity tests.
- More than 10% of the eight surrounding pixels in a 3 x 3-pixel segment are clear.
- A cloud detection test shows no cloudy pixels other

than those found in a spatial uniformity test for the eight surrounding pixels in a 3 x 3-pixel segment.

The fourth filter changes isolated cloudy pixels as identified in a cloud detection test using band 7 (3.9 μm) data to clear. Band 7 data have lower SNR values than others. This filter corrects misclassification caused by this uncertainty. If the following conditions are satisfied, the pixel is marked as clear:

- The pixel is cloudy as determined in tests related to 3.9 μm data. (Gross test of 3.9 μm reflectance (Section 2.4.3); second, third and fourth top emissivity tests (Section 2.4.4); third cloud absorption test (Section 2.4.5).)
- All eight surrounding pixels in a 3x3-pixel segment are clear.

The fifth filter changes isolated clear pixels to cloudy. If the following conditions are satisfied, the pixel is classified as cloudy:

- The pixel is clear.
- All eight surrounding pixels in a 3 x 3-pixel segment are cloudy.

2.4.10 Detection of cloudy-clear mixed situations

Cloudy pixels are classified as either cloudy or cloudy-clear mixed. If the following condition is satisfied, the pixels is marked as cloudy-clear mixed:

$$T_{10.4} - T_{12.4} \geq 2.0 \tag{87}$$

If the following condition is satisfied, the pixel is classified as cloudy:

$$T_{10.4} - T_{12.4} < 2.0 \tag{88}$$

2.4.11 Aerosol detection

For products derived with clear pixels such as SST and CSR, CMP needs to detect all objects that block radiative transfer from surface to satellite except for the atmosphere. As aerosols may go undetected in cloud mask tests, a volcanic ash detection algorithm (Pavolonis et al. 2009) consisting of a detection part, a confidence setting part and a confidence adjustment part is used.

The conditions for aerosol detection are as shown below. Examples of variables for aerosol detection are given in Figure 4.

$$\varepsilon_{11.2}^{stropo} \geq 0.02 \tag{89}$$

$$\varepsilon_{8.6}^{stropo} \geq 0.02 \tag{90}$$

$$0.0 < \beta_{12.4/11.2}^{stropo} < 1.0 \qquad (91)$$

$$0.0 < LRC(\beta_{12.4/11.2}^{stropo}) < 1.0 \qquad (92)$$

$$0.0 < \beta_{8.6/11.2}^{stropo} < 10.0 \qquad (93)$$

$$0.0 < LRC(\beta_{8.6/11.2}^{stropo}) < 10.0 \qquad (94)$$

The confidence information is set using C_{PIX}, C_{LRC} and C_{SUM} as confidence flags. Three grades of confidence (0: high; 1: moderate; 2: non-ash) are set for C_{PIX} and C_{LRC} based on the conditions for the variables $(\beta_{8.6/11.2}^{stropo}, \beta_{12.4/11.2}^{stropo})$ and $(LRC(\beta_{8.6/11.2}^{stropo}), LRC(\beta_{12.4/11.2}^{stropo}))$, respectively. The conditions are summarized in Figure 5. The red area is high, the orange area is moderate, the green area is moderate if $\varepsilon_{11.2}^{stropo} > 0.10$ and non-ash if

$\varepsilon_{11.2}^{stropo} \leq 0.10$, and the white area is non-ash confidence.

C_{SUM} is a summation of C_{PIX} and C_{LRC} for five grades of confidence {0: high; 1: moderate; 2: low; 3: very low, 4: non-ash}.

Confidence adjustment involves nine processes performed successively from A to I as summarized in Table 7.

Pixels with high and moderate confidence C_{SUM} are set as aerosol areas with high and low quality, respectively, in CMP output (Table 3). An example of aerosol detection is shown in Figure 6. The leftmost part shows plots in an HSD line pixel grid. The center and rightmost parts are 2D plots similar to those in Figure 5 showing the detection conditions. These figures indicate correspondence between the cloud area and detection conditions.
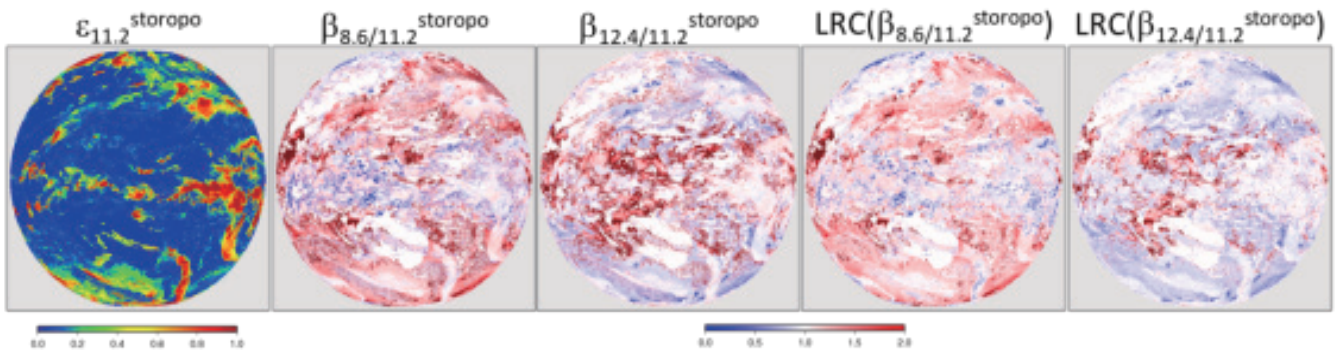

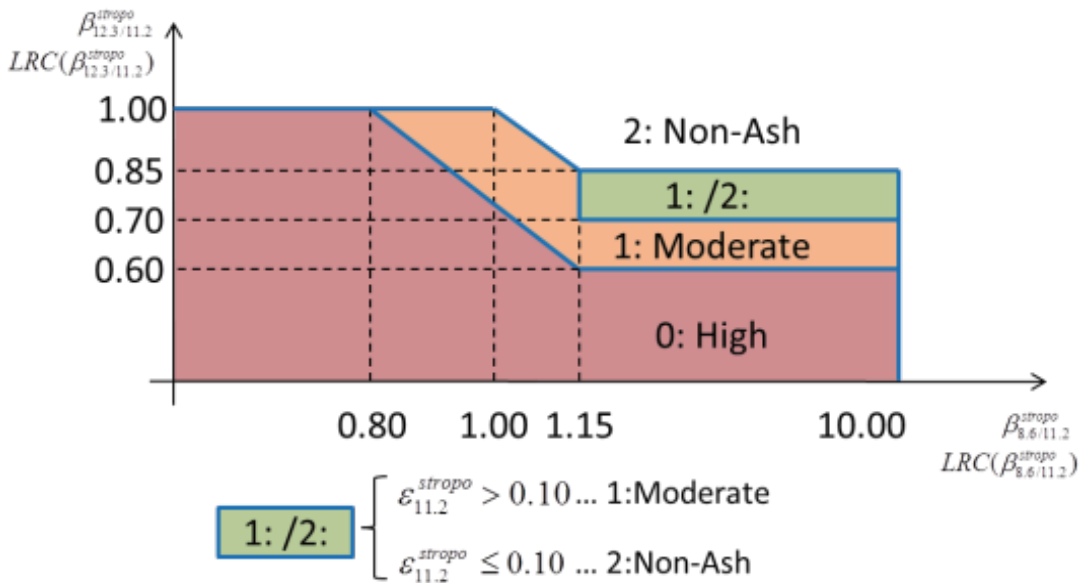Fig.4 Examples of aerosol detection variables for 02 UTC on 21st Mar. 2015

Fig.5 Conditions for setting of the three confidence grades for 02 UTC on 21 Mar. 2015

Table 7 Confidence adjustment

|	Conditions	Adjustment
A	$\varepsilon_{8.5}^{stropo} > \varepsilon_{11.2}^{stropo}$ $\varepsilon_{7.4}^{stropo} > \varepsilon_{8.5}^{stropo}$ $T_{11.2} - T_{12.4} < 0.0$	If $C_{SUM} = 2$, set $C_{SUM} = 1$ If $C_{PIX} = 0$, set $C_{SUM} = 1$ If $C_{PIX} = 1$ and $C_{LRC} = 2$ set $C_{SUM} = 1$ If $C_{SUM} = 4$ set $C_{SUM} = 3$
B	$\varepsilon_{8.5}^{stropo} > \varepsilon_{11.2}^{stropo}$ $T_{11.2} - T_{12.4} < -0.75$	If $C_{SUM} = 2$, $C_{PIX} < 2$ and $C_{LRC} = 2$ set $C_{SUM} = 1$ If $C_{SUM} = 4$, set $C_{SUM} = 3$
C	$T_{11.2} - T_{12.4} < 1.0$	If $C_{PIX} = 0$, set $C_{SUM} = 1$ If $C_{PIX} = 1$ and $C_{LRC} = 2$, set $C_{SUM} = 1$
D	$T_{11.2} - T_{12.4} < -0.75$	If $C_{SUM} < 2$ and $C_{PIX} < 2$, set $C_{SUM} = 1$ If $C_{SUM} < 2$ and $C_{LRC} < 2$, set $C_{SUM} = 1$
E	$T_{11.2} - T_{12.4} < \begin{cases} -0.5 & ; -1.0 \times 10^6 < \varepsilon_{11.2}^{stropo} - \varepsilon_{12.4}^{stropo} \\ -0.75 & ; -1.0 \times 10^3 < \varepsilon_{11.2}^{stropo} - \varepsilon_{12.4}^{stropo} \le -1.0 \times 10^6 \\ -1.0 & ; \varepsilon_{11.2}^{stropo} - \varepsilon_{12.4}^{stropo} \le -1.0 \times 10^3 \end{cases}$	If $C_{SUM} = 4$, set $C_{SUM} = 3$
F	$\varepsilon_{11.2}^{stropo} < 0.05$	If $C_{SUM} = 0$, set $C_{SUM} = 1$
G	$\varepsilon_{11.2}^{stropo} > 0.5$ $0 < \beta_{7.3/11.2}^{stropo} < 1$ $\beta_{12.4/11.2}^{sopaque} \ge 1$	If $C_{SUM} = 0$, set $C_{SUM} = 4$
H	$\theta_{satZ} > 80.0$	Set $C_{SUM} = 4$
I	$75.0 \le \theta_{satZ} \le 80.0$ $\beta_{12.4/11.2}^{stropo} > -0.01 \cdot \theta_{satZ} + 1.6$	Set $C_{SUM} = 4$
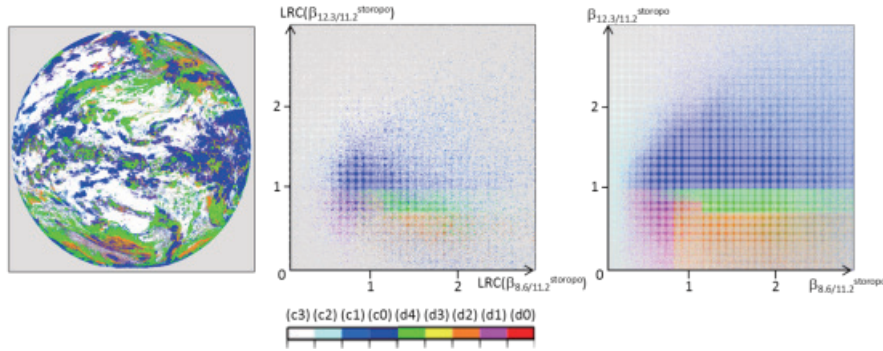
Fig. 6 Example of aerosol detection (left), $(LRC(\beta_{8.6/11.2}^{stropo}), LRC(\beta_{12.4/11.2}^{stropo}))$ space (center) and $(\beta_{8.6/11.2}^{stropo}, \beta_{12.4/11.2}^{stropo})$ space (right). The data (c0) – (c3) and (d0) – (d4) plotted in each color are: (c3): no conditions met; (c2): only $\varepsilon_{11.2}^{stropo}$ condition met; (c1): only $\varepsilon_{8.6}^{stropo}$ condition met; (c0): $\varepsilon_{11.2}^{stropo}$ and $\varepsilon_{8.6}^{stropo}$ conditions met; (d4): identified as non-ash quality; (d3): identified as very low quality; (d2): identified as low quality; (d1): identified as moderate quality (d0): identified as high quality. The scene is for 02 UTC on 21 Mar. 2015.

2.5 Offsets

To compensate for the uncertainty of clear sky data in radiative transfer calculation, offsets are added as additional terms for main variable thresholds in cloud mask tests. The offsets are determined by making the pre-final cloud mask similar to the actual cloud mask. It is desirable to use a low-earth-orbit satellite cloud product as actual cloud mask data because of their high quality and rich data content. This type of cloud mask is based on the Aqua/MODIS cloud mask product as actual data. Offsets are set for five surfaces (sea, land, snow/sea ice, sand and vegetation), two sun zenith angle conditions ($\theta_{sunZ} < 90$ deg., 90 deg. $\leq \theta_{sunZ}$) and four satellite zenith angle conditions ($\sec(\theta_{satZ}) < 3$, $3 \leq \sec(\theta_{satZ}) < 5$, $5 \leq \sec(\theta_{satZ}) < 7$, $7 \leq \sec(\theta_{satZ})$). To reduce the effect of approximation in radiative transfer calculation, offsets depending on several conditions are used.

As it is practically impossible to tune the offsets for each cloud mask test independently, the NOAA/NESDIS method (Heidinger and Straka III 2012) is adopted. Cloud mask tests are essentially used for cloud detection and contain an "or" condition for the result of the pre-final cloud mask. Accordingly, misclassification of cloudy as clear (B in Table 8) in one test can be remedied by cloud detection in another, while misclassification of clear as cloudy (C in Table 8) will result in false cloud

detection in the pre-final cloud mask. A low ratio of false alarms for cloudy conditions is therefore desirable.

First, offsets resulting in ratios of 0.005, 0.01, 0.02, 0.04, 0.06, 0.08, 0.1, 0.12, 0.15, 0.2, 0.3, 0.5, 0.8 and 0.99 for false alarms of cloudy conditions in each cloud mask test are calculated. In the relevant test, the offset value is discretized and a histogram showing numbers of clear pixels in actual cloud mask data is created. A cumulative histogram is made by gathering histogram data from a cloudy-side discretized bin. By normalizing the cumulative histogram based on the total number of clear pixels and subtracting the result from 1, ratios of false alarms for cloudy conditions in each discretized bin are calculated as per the green line shown in Figure 7. Following the dataset of false alarm ratios from the cloudy-side discretized bin, offset values corresponding to the first discretized bin with ratios of more than 0.005, 0.01, 0.02, 0.04, 0.06, 0.08, 0.1, 0.12, 0.15, 0.2, 0.3, 0.5, 0.8 and 0.99 for false alarms of cloudy conditions are derived.

Second, the hit ratio (see Table 8) of the pre-final cloud mask for each ratio of false alarms for cloudy conditions is calculated. An offset corresponding to the false alarm ratio for cloudy conditions with the maximum hit ratio of the pre-final cloud mask (with the condition that the ratio is lower than 0.3) is adopted.
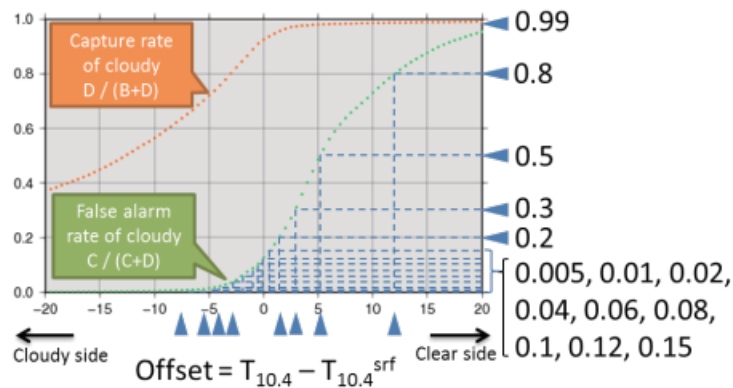

Fig. 7 Example of false alarm ratios for cloudy conditions in a top temperature test for land

Table 8 Hit ratio definition

		Actual cloud mask	
		Clear	Cloudy
CMP	Clear	A	B
	Cloudy	C	D

Hit ratio = (A + D) / (A + B + C+ D)

Clear hit ratio = A / (A + B)

Cloudy hit ratio D / (C + D)

2.6 Quality information

Two grades are used to express cloud mask quality for each of clear and cloudy pixels (i.e., high-quality clear, low-quality clear, high-quality cloudy and low-quality cloudy). Low quality is assigned to filtered pixels regardless of their clear or cloudy status, while quality for non-filtered pixels is based on the safety margin. For cloudy pixels, high quality is assigned if the difference between the observation value and the threshold of the main variables in the last test is greater than the safety margin. For clear pixels, high quality is assigned if the differences between the observation value and the threshold of the main variables in all tests are greater than the safety margin.

The safety margin for snow/sea ice detection is set as $0.2 \times R_{1.6}^{srf}$ for testing of variable $R_{1.6}$. Calculation of the safety margin for a test with an offset is similar to calculation of the offset based on the false alarm ratio for cloudy conditions. To avoid confusion, the offset described in the previous subsection is referred to as the all-sky offset, and this offset plus a safety margin for clear sky or cloudy conditions is referred to as the clear-sky offset or the cloudy offset. While the all-sky offset is calculated to maximize the hit ratio (see Table 8) of the pre-final cloud mask, the clear-sky offset is calculated to maximize the clear hit ratio (see Table 8)

with a constraint to avoid detection with an extremely biased ratio of clear-sky and cloudy pixels. The constraint requires that the number of clear-sky pixel hits in cloud mask results obtained using a clear-sky offset should be greater than 0.8 times that obtained using an all-sky offset. The cloudy offset is calculated in the same way with the clear sky offset but to maximize the cloudy hit ratio (see Table 8). Correspondence between the three offsets and cloud mask quality information is shown in Figure 8.

3. Results

3.1 Output example

An example of CMP output for 02 UTC on 30 Mar. 2015 is shown in Figure 9.

A comparison of CMP with clear, all-sky and cloudy offsets against the MODIS cloud product is shown in Figure 10. The clear offset produces more cloudy pixels with MODIS clear detection (cyan points) than the others, and the cloudy offset produces more clear pixels with MODIS cloud detection (red points) than the others. The result produced with the all-sky offset is more consistent in the MODIS result than the others. In these scenes, the hit ratio (see Table 8) is 83.2% for the clear-sky offset, 85.6% for the all-sky offset and 80.6% for the cloudy-sky offset.
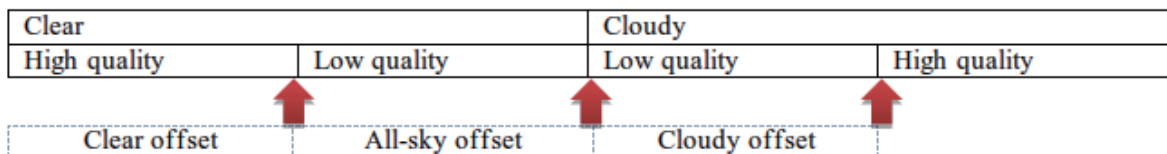

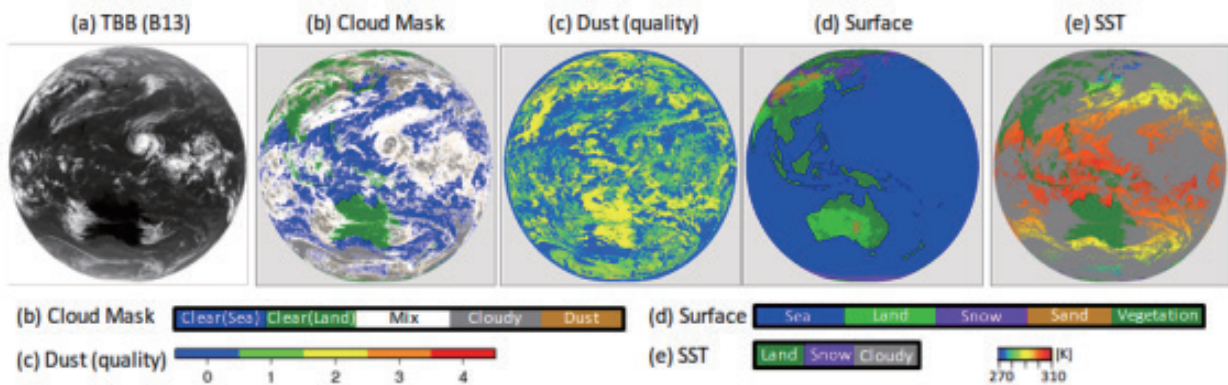Fig. 8 Correspondence between the three offsets and cloud mask quality information

Fig. 9 (a) Brightness temperature in B13, (b) cloud mask, (c) aerosol detection, (d) surface information and (e) SST used for cloud mask at 02 UTC on 30 Mar. 2015
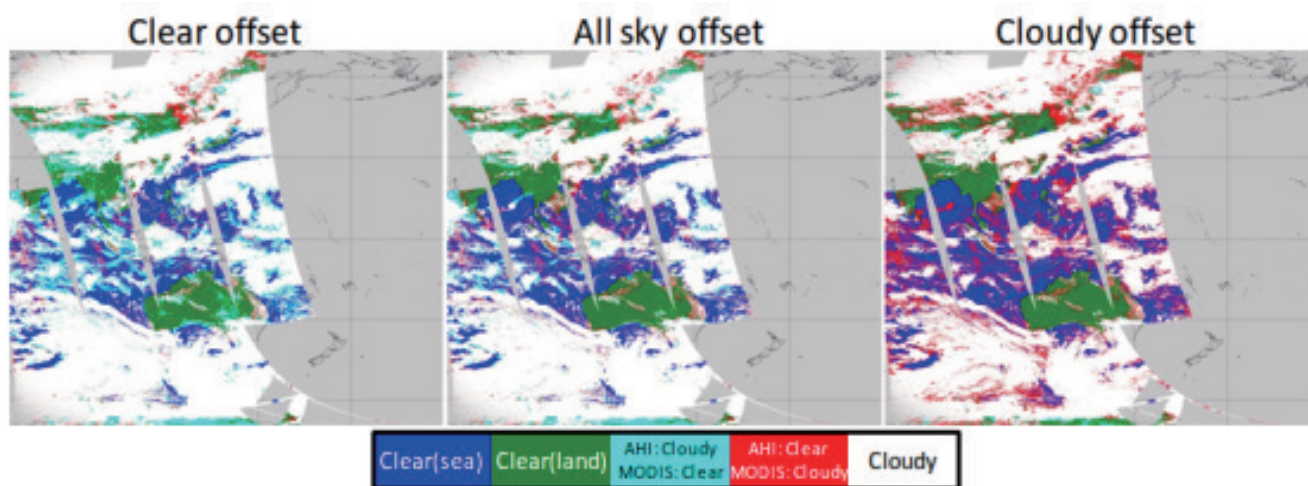
Fig. 10 Comparison of CMP with clear offset (left), all-sky offset (center) and cloudy offset (right) against the MODIS cloud product in scenes from 00 UTC to 09 UTC on 17 Mar. 2015

3.2 Long-term evaluation

The CMP algorithm was applied to Meteosat Second Generation (MSG)/Spinning Enhanced Visible and InfraRed Imager (SEVIRI) data for long-term evaluation. As evaluation periods, two weeks from each season were selected (i.e., 28 December 2011 – 10 January 2012, 28 March – 10 April 2012, 27 June – 10 July 2012 and 27 September – 10 October 2012). Table 9 shows the resulting hit ratios compared with those of the Aqua/MODIS product. The value was consistent at around 85% for all seasons.

Table 9 Hit ratios of the CMP algorithm for MSG/SEVIRI data compared with those of the Aqua/MODIS product for each season (winter: 28 December 2011 – 10 January 2012; spring: 28 March – 10 April 2012; summer: 27 June – 10 July 2012; autumn: 27 September – 10 October 2012)

	Winter	Spring	Summer	Autumn	All
All region	0.86	0.85	0.85	0.85	0.85
Sea	0.86	0.85	0.85	0.86	0.85
Snow/Ice	0.86	0.81	0.72	0.86	0.81
Sand	0.87	0.86	0.86	0.89	0.87
Vegetation	0.86	0.84	0.83	0.83	0.84
Others	0.80	0.82	0.86	0.84	0.84

4. Summary

MSC's Himawari-8 cloud mask product (CMP) has been produced since Himawari-8 began operation in July 2015. The CMP algorithm involves snow/sea ice detection, cloud detection, filtering and aerosol detection based on an algorithm proposed by NWC-SAF and NOAA-NESDIS. Most of the cloud detection tests used involve threshold methods based on radiative transfer calculation using NWP data for atmospheric profiles. The thresholds are modified using offsets determined based on comparison with the MODIS cloud mask product. The initial results showed that the CMP hit ratio derived from such comparison was more than 85%. Application of the CMP algorithm to SEVIRI data showed that hit ratios were around 85% for all seasons.

Acknowledgement

Reference

Aoki, T., M. Fukabori and A. Uchiyama, 1999: Numerical Simulation of the Atmospheric Effects on

Snow Albedo with a Multiple Scattering Radiative Transfer Model for the Atmosphere-Snow System, Journal of the Meteorological Society of Japan, Vol. 77, No. 2, 595-614

Bessho, K., K. Date, M. Hayashi, A. Ikeda, T. Imai, H. Inoue, Y. Kumagai, T. Miyakawa, H. Murata, T. Ohno, A. Okuyama, R. Oyama, Y. Sasaki, Y. Shimazu, K. Shimoji, Y. Sumida, M. Suzuki, H. Taniguchi, H. Tsuchiyama, D. Uesawa, H. Yokota, and R. Yoshida, 2016: An introduction to Himawari-8/9 - Japan's new-generation geostationary meteorological satellites. J. Meteor. Soc. Japan, 94, doi:10.2151/jmsj.2016-009.

Cox, C. and W. Munk, 1954: Measurement of the roughness of the sea surface from photographs of the sun's glitter, J. Opt. Soc. Amer., 44(n), 838-850.

Eyre, J.R., 1991: A fast radiative transfer model for satellite sounding systems. ECMWF Tech. Memo. 176, 28pp

Heidinger, A. and W. C. Straka III, 2012: Algorithm Theoretical Basis Document ABI Cloud Mask. Available at http://www.star.nesdis.noaa.gov/goesr/docs/ATBD/Cloud_Mask.pdf.

Kurihara, Y., T. Sakurai, and T. Kuragano, 2006: Global daily sea surface temperature analysis using data from satellite microwave radiometer, satellite infrared radiometer and in-situ observations. Sokko Jiho, 73, 1-18 (in Japanese).

Li, J. and K. Shibata, 2006: On the Effective Solar Pathlength. Journal of the Atmospheric Sciences 2006 63:4, 1365-1373

Meteo-France, 2012: Algorithm Theoretical Basis Document for "Cloud Products" (CMa-PGE01v3.2, CT-PGE02 v2.2 & CTTH-PGE03 v2.2). Available at http://www.nwcsaf.org/indexScientificDocumentation.html.

Mouri, K., T. Izumi, H. Suzue, and R. Yoshida, 2016a: Algorithm Theoretical Basis Document of Cloud Type/Phase Product. Meteorological Satellite Center Technical Note, 61, 19-31.

Mouri, K., H. Suzue, R. Yoshida, and T. Izumi, 2016b: Algorithm Theoretical Basis Document of Cloud top height product. Meteorological Satellite Center Technical Note, 61, 33-42.

Nakajima, T. and M. Tanaka, 1986: Matrix formulation for the transfer of solar radiation in a plane-parallel scattering atmosphere, J. Quant. Spectrosc. Radiat. Transfer, 35, 13-21.

Okawara, N., Y. Yoshizaki and M. Tokuno, 2003: Development of Aerosol Products from GMS/VISSR and NOAA/AVHRR Image Data, Meteorological Satellite Center Technical Note, 42, 43-52 (in Japanese).

Pavolonis, M, and J. Sieglaff, 2009: GOES-R Advanced Baseline Imager (ABI) Algorithm Theoretical Basis Document for Volcanic Ash (Detection and Height). Available at http://www.star.nesdis.noaa.gov/goesr/docs/ATBD/VolAsh.pdf.

Roujean, J.-L., M. Leroy, and P. Y. Deschamps, 1992: A bidirectional reflectance model of the Earth's surface for the correction of remote sensing data, J. Geophys. Res., 97, 20455-20468.

Strahler, A. H., J.-P. Muller, MODIS Science Team Members, 1999: MODIS BRDF/Albedo Product: Algorithm Theoretical Basis Document Version 5. Available at http://modis-land.gsfc.nasa.gov/brdf.html.

Tokuno, M., 2002: Advanced Satellite Cloud Grid Information Data, Meteorological Satellite Center Technical Note,40, 1-24 (in Japanese).

Uesawa, D., 2009: Clear Sky Radiance (CSR) Product from MTSAT-1R, Meteorological Satellite Center Technical Note, 52, 39-48.

Yasuda, H., Y. Shirakawa, 1999: Improvement of the Derivation Method of Sea Surface Temperature from GMS-5 Data, Meteorological Satellite Center Technical Note, 37, 19-33 (in Japanese).

ひまわり 8 号 雲マスクプロダクト

今井　崇人*、吉田　良**

要旨

　本誌は、気象衛星センターで開発された、ひまわり 8 号雲マスクプロダクト（CMP）の算出アルゴリズムの詳細を記述したものである。CMP は、ひまわり 8 号基本雲プロダクト（雲タイプ、雲相、雲頂高度を含む）の一部であり、2015 年 7 月 7 日から正式運用されている。

　CMP のアルゴリズムは、NWC-SAF と NOAA/NESDIS がそれぞれ MSG/SEVIRI と GOES-R/ABI 用に開発した雲マスクアルゴリズムに基づく、閾値を用いた複数の雲検出テストによるものである。これらの閾値は、数値モデルデータを入力とした放射伝達計算によって決定された後、MODIS の雲マスクプロダクトとの比較によって決定されるオフセットによって修正されたものである。CMP の初期結果を MODIS プロダクトと比較した結果、適中率は 85 ％以上であることが示された。また、本アルゴリズムを SEVIRI データに適用した結果、四季を通じて適中率が 85 ％程度であることがわかった

＊ 気象庁観測部観測課観測システム運用室
＊＊ 気象衛星センターデータ処理部システム管理課